Title

Flow boiling heat transfer in a helically coiled steam generator for nuclear power applications

Authors & Affiliations

Lorenzo Santini

ENEL Ingegneria e Ricerca SpA, Via Mantova 24, 00198 Roma, Italy, Tel: +421 366 378 654, e-mail: lorenzo.santini@enel.com

Andrea Cioncolini

School of Mechanical, Aerospace and Civil Engineering, University of Manchester, George Begg Building, M1 3BB Manchester, United Kingdom, Tel: +44.161.306.3711, e-mail: andrea.cioncolini@manchester.ac.uk

Matthew T. Butel

School of Physics and Astronomy, University of Manchester, Oxford Road, M13 9PL Manchester, United Kingdom. *Current address*: BAE Systems Marine Limited, Warwick House, PO Box 87, Farnborough Aerospace Centre, GU14 6YU Farnborough, United Kingdom, e-mail: matthew.butel@baesystems.com

Marco E. Ricotti

Department of Energy, Politecnico di Milano, Via La Masa 34, 20156 Milano, Italy, Tel: +39 02 2399 6325; e-mail: marco.ricotti@polimi.it

Abstract

Forced convection boiling of water was experimentally investigated in a 24 m long full-scale helically coiled steam generator tube, prototypical of the steam generators with in-tube boiling used in small modular nuclear reactor systems. Overall, 1575 axially local and peripherally averaged heat transfer coefficient measurements were taken, covering operating pressures in the range of 2 to 6 MPa, mass fluxes from 200 to 800 $kgm^{-2}s^{-1}$ and heat fluxes from 40 to 230 kWm^{-2}. The heat transfer coefficient was found to depend on the mass flux and on the heat flux, indicating that both nucleate boiling and convection are contributing to the heat transfer process. Seven widely quoted flow boiling correlations for straight tubes fitted the present helical coil databank with a mean absolute percentage error within 15-20%, which was comparable with the experimental uncertainty of the

measured heat transfer coefficient values, thus indicating that curvature effects on flow boiling are small and negligible in practical applications.

Keywords

Helical coil; Convective flow boiling; Steam generator; Curvature effect; Small modular nuclear reactor;

1. Introduction

Helically coiled tubes have many advantages over conventional straight tubes that make them extensively used in steam generators and heat transfer equipment in chemical plants, refrigeration systems, power stations and nuclear reactors. For example, they provide a greater heat transfer area per unit volume, which make them attractive in applications where compactness is required, such as marine propulsion and integral layout nuclear reactors. In addition, helically coiled tubes are less susceptible to problems associated with thermal expansion, which can present operational constraints on straight tube systems operating at high temperature. Moreover, the large radial accelerations induced by the helical path maintain the tube internal surface wet to higher vapor qualities than in a straight pipe, thus delaying dryout and the associated degradation in the heat transfer coefficient, and also improve the heat transfer effectiveness after dryout promoting de-entrainment of the liquid droplets from the vapor. Recently, helically coiled steam generators are receiving renewed interest, promoted by their frequent use in advanced small modular nuclear reactor systems. According to the International Atomic Energy Agency [1], nuclear reactors are classified as small modular reactors when their equivalent electric power output is less than 300 MW. A recent review [2] identified more than 45 different small modular reactor designs in various stages of development, including advanced water cooled reactors, high temperature gas cooled reactors, liquid metal cooled reactors and molten salt reactors. The modular approach of advanced small modular reactor systems offers many advantages over traditional nuclear power plants, including lower initial capital investment, simplified design, economy of mass production, enhanced passive safety and proliferation resistant features [3]. In addition, the modular concept provides greater flexibility, enabling small modular reactor systems to meet much smaller local demands for power [4]. The most mature small modular reactor designs with the potential for near- and mid-term commercial deployment are the integral pressurized water reactor designs, which house all the components usually associated with the primary circuit of a pressurized water reactor within a single reactor vessel. They are considered to pose the lowest technical risk, since they combine proven technologies and many years of commercial operating experience with traditional pressurized water reactors,

with a range of novel components and innovative design features that enhance the safety of the reactor [5]. Integral layout, pressurized water nuclear reactors are typically equipped with helically coiled steam generators, notably for their compactness, heat transfer efficiency and low susceptibility to thermal expansion concerns. Due to its practical relevance, flow boiling in helically coiled tubes has been investigated quite extensively [6-12], showing that the heat transfer over most of the vapor quality range is due to both nucleate boiling and convection. Most authors found straight tube flow boiling correlations appropriate to predict the heat transfer coefficient during flow boiling in helically coiled tubes, although a general consensus on which straight tube correlations work best for helical coils has not been reached. Remarkably, some authors found straight tube flow boiling correlations not very accurate for helical coils [9,10], and proposed new correlations specific for flow boiling in helically coiled tubes. Notably, most of the available experimental studies have been carried out with comparatively short test sections, while the measurements taken with long, prototypical test sections that are required for the validation of system computer codes used in design, optimization and transient and safety analysis are still missing. To fill in this gap, the present study was conducted with a prototypical, full-scale 24 m long steam generator test tube, covering the operating conditions of medium pressure (2-6 MPa), low mass flux (200-800 $kgm^{-2}s^{-1}$) and low heat flux (40-230 kWm^{-2}) typical of the steam generators used in small modular nuclear reactor power plants. Moreover, this study includes an extensive assessment of 11 straight tube flow boiling correlations regarding their suitability for helically coiled tubes, using the large databank generated herein (1575 points). This study is part of a wide experimental program addressing single and two-phase boiling flows in helical coils, targeting specifically the design and operation of compact steam generators for nuclear power applications, notably small modular units [13-18].

2. Experiments

The test section used for the present experimental campaign was an helically coiled steam generator tube, made of stainless steel AISI 316 and framed into an open loop test facility built inside the boiler building of the "Emilia" power station in Piacenza-Italy (SIET Labs: www.siet.it), as shown schematically in Figs. 1 and 2. The test tube had internal and external diameters of 12.49 mm and 17.23 mm, respectively (corresponding nominal values were 12.53 mm and 17.15 mm), and a total length of 32 meters. In particular, five tubes of 6 meters each and one tube of 2 meters were coiled and welded together to compose the test section tube. The variation of the tube external diameter along the test section due to the bending was found to be within 1-2%, small enough to neglect the tube ovalization in the data reduction and post processing. The average roughness of the tube inner

surface was 3.1 μm (from six local measurements: maximum value 3.5 μm, minimum value 2.5 μm). The coil diameter and coil pitch were 1.0 m and 0.79 m, respectively, corresponding to 10 full coil turns and resulting in a total height of the steam generator tube of 8.0 m. The geometry of the test tube is fairly prototypical of steam generators for small modular pressurized water nuclear reactors of integral layout. The test section main geometrical data are summarized in Table 1.

As shown in Fig. 1, the test facility supply section fed the test section with demineralized, deionized water (mean electrical conductivity of 1.5 μScm^{-1}) from a reservoir by means of a booster pump and a feed-water pump in series. The bypass line with a control valve located downstream of the pumps allowed the adjustment of the flow rate to the test section. A throttling valve was also included to avoid dynamic instabilities (density wave type) in the test section during operation. The subcooling of the water feeding the test section was adjusted with an electrical pre-heater located upstream of the test section (within 40-50 K in the present experiments). The test section was electrically heated via Joule effect with DC current. In particular, as shown in Fig. 2, three electrical power connections were provided: one at the inlet of the test section, one at the outlet of the test section and another one at an intermediate position along the test tube, located 24 m from the inlet and 8 m from the outlet of the test section. This allowed the heat flux in the last 8 m long portion of the test section to be varied independently from the heat flux delivered in the first 24 m long portion of the test tube, a feature that proved useful during post dryout studies (not discussed here) to better mimic the heat flux profile of actual steam generators, which are fluid heated configurations. During the experiments reported and discussed here, however, the last 8 m long portion of the test section was not powered and was always kept adiabatic, and only the first 24 m long portion of the test tube was heated with uniform heat flux. All the experimental results discussed here, therefore, were generated in the first 24 m long portion of the test tube and refer to convective flow boiling conditions prior to the dryout, with electrical heating and uniform heat flux along the test tube. As shown in Fig. 2, three valves (two automatically air operated and one manual) located at the test section discharge allowed adjustment of the operating pressure in the test section.

The mass flow rate through the test section was measured with a Coriolis flow-meter (uncertainty within ± 1%). The absolute pressure at the inlet of the test section was measured with an absolute pressure transducer (uncertainty within ± 0.1%). As shown in Fig. 2, nine pressure taps were evenly distributed along the test tube and eight differential pressure transducers (uncertainty within ± 0.4%) were connected to these pressure taps. This allowed a fairly accurate reconstruction of the pressure profile along the test section, which is crucial to get an accurate estimate of the local fluid saturation temperature needed to calculate the local heat transfer

coefficient. It is worth noting that the measured two-phase pressure drops are discussed in Santini et al. [17], while the focus of the present study is the heat transfer coefficient during flow boiling. The heated tube external temperature was measured with 76 K-type thermocouples (uncertainty within ± 0.5 K), distributed along the first 24 m long portion of the test tube at 21 axial stations, each counting 2 or 4 thermocouples evenly distributed around the tube periphery. The water bulk temperature at the inlet of the test section was measured with a K-type thermocouple located inside a small well (uncertainty within ± 0.5 K). All instruments were off-line calibrated prior to the experiments with the exception of the tube wall thermocouples, which were end-to-end on-line calibrated in dedicated pre-tests with adiabatic two-phase flow. The heated tube was thermally insulated with rock wool. The thermal losses of the test tube to the environment were measured with dedicated single-phase flow pre-tests, and properly accounted for in the successive two-phase flow data reduction (the thermal losses were within 3-4% of the total Joule heating power during flow boiling experiments). The heated tube internal temperature was deduced from the external temperature measurements assuming one-dimensional heat conduction through the tube thickness and uniform heat generation. At each thermocouple axial station the internal temperatures of the tube were averaged out to yield the tube average internal temperature. The peripherally averaged, axially local heat transfer coefficient was calculated from the heat flux (deduced from the measurement of the electric current flowing through the tube thickness and from the measurement of the voltage drop across the heated tube, and taking into account the thermal losses of the heated tube) and from the temperature difference between the tube (average internal temperature) and the bulk fluid (deduced from the measured pressure profile using the water saturation curve). The angular variation around the tube perimeter of the heat transfer coefficient was therefore not addressed in the present study.

The test apparatus was validated with preliminary experiments carried out with water in single-phase flow conditions. The measured heat transfer coefficient values are compared in Fig. 3 with the predictions of the following correlation proposed by Gnielinski [19] for single-phase flow through helical coils:

$$Nu = \frac{(f/8)\,\mathrm{Re}\,\mathrm{Pr}}{1+12.7\sqrt{(f/8)}\left(\mathrm{Pr}^{2/3}-1\right)}\left(\frac{\mathrm{Pr}}{\mathrm{Pr}_w}\right)^{0.14} \quad for \quad \mathrm{Re} > 2.2\cdot 10^4 \tag{1}$$

where the friction factor f for turbulent flow in helical coils is predicted as:

$$f = \left[0.3164\,\mathrm{Re}^{-0.25} + 0.03\left(\frac{d}{D}\right)^{0.5}\right]\left(\frac{\mu_w}{\mu}\right)^{0.27} \tag{2}$$

where Re and Pr are the Reynolds and Prandtl numbers, d is the tube inner diameter, D is the coil diameter and μ is the fluid viscosity, all calculated at the fluid bulk temperature with the exception of Pr_w and μ_w which are

calculated at the tube inner surface temperature. The Reynolds number range covered in the single-phase flow validation experiments was 2.4 10^4-1.0 10^5, well within the limits of applicability of Eq. (1). As can be seen in Fig. 3, the agreement between measurements and predictions is satisfactory.

3. Results and discussion

Results from a typical experimental run are displayed in Fig. 4, where the pressure profile (top), the temperature profiles (middle) and the heat transfer coefficient profile (bottom) are displayed versus the axial position along the test tube. The heat transfer coefficient profile in Fig. 4 (bottom) is also displayed as a function of the vapor quality. As can be seen in Fig. 4 (top), there is a noticeable reduction in pressure at the very beginning of the test tube due to inlet effects. Further along the test tube, the pressure gradient gradually increases as the fluid progressively evaporates and accelerates, as shown by the downward curvature of the pressure profile. The fluid temperature in saturated flow conditions (Fig. 4 middle) is deduced from the measured pressure profile, using the fluid saturation curve (NIST REFPROP). The mild reduction of the fluid saturation temperature along the test tube is due to the local pressure reduction, while the decrease of the tube wall temperature follows both the reduction of the fluid saturation temperature and the local variation of the heat transfer coefficient. Finally, the heat transfer coefficient in Fig. 4 (bottom) increases as the fluid gradually evaporates along the test tube and the local vapor quality increases.

Experiments were carried out with operating pressures in the range of 2 to 6 MPa, mass fluxes from 200 to 800 $kgm^{-2}s^{-1}$ and heat fluxes from 40 to 230 kWm^{-2}, which cover the operating conditions of low-medium pressure, low mass flux and low heat flux typical of the steam generators with in-tube boiling used in small modular nuclear reactor power plants. Overall, 1575 heat transfer coefficient measurements were collected (uncertainty within 5-20%, with most measurements in the range of 10-20%), and all these measurements are peripherally averaged and axially local along the test tube. Selected histograms that further describe the collected data are shown in Fig. 5.

Selected measurements that show the dependence of the heat transfer coefficient on the mass flux, the heat flux and the operating pressure are shown in Figs. 6 and 7, where the measured heat transfer coefficient values are displayed versus the local vapor quality with mass flux, heat flux and operating pressure as parameters. As can be seen in Fig. 6, at the lowest mass flux and heat flux values tested the heat transfer coefficient is fairly constant and independent of the local vapor quality, suggesting that forced convection effects are small and wall nucleation is therefore controlling the heat transfer process. At higher mass flux and heat flux values, however,

the heat transfer coefficient increases with an increase of the vapor quality, indicating that forced convection effects gradually come into play as the mass flux is increased. The measurements displayed in Fig. 6 refer to the highest operating pressure tested in the present study, corresponding to 6 MPa. It is revealing to compare the heat transfer coefficient measurements in Fig. 6 obtained at the lowest mass flux and heat flux values (mass flux: 200 $kgm^{-2}s^{-1}$, heat flux: 46 kWm^{-2}) with the heat transfer coefficient profile displayed in Fig. 4 (bottom), measured at similar values of the mass flux and heat flux (mass flux: 206 $kgm^{-2}s^{-1}$, heat flux: 51 kWm^{-2}) but with a lower operating pressure of 2 MPa. It is evident that at the lower operating pressure of 2 MPa convective effects are clearly present, as the heat transfer coefficient increases with an increase of the vapor quality, while convective effects are no longer present at the higher operating pressure of 6 MPa, as the heat transfer coefficient no longer depends on the vapor quality. This can be interpreted considering that an increase of the operating pressure causes the vapor density to increase, and this in turns yields a deceleration of the flow, and correspondingly a reduction of convective effects. As such, in the present study both forced convection and wall nucleation seem to affect the measured heat transfer coefficient, with wall nucleation playing a dominant role at very low mass flux, very low heat flux and high operating pressure. Consistently, as shown in Fig. 7, an increase of the operating pressure yields a decrease of the heat transfer coefficient, as the increase of the vapor density that follows the increase of the operating pressure yields a reduction of the average velocity of the flow, which in turn weakens convective effects, while the enhanced wettability induced by the higher pressure reduces the bubbling activity at the tube wall. These trends are fairly typical of in-tube flow boiling in helical coils at low mass flux and low heat flux, and are in agreement with the findings of Owhadi et al. [6], Zhao et al. [9] and Hwang et al. [12].

The measured heat transfer coefficients are compared with the predictions of several widely quoted empirical correlations (Chen [20]; Shah [21]; Gungor and Winterton [22,23]; Liu and Winterton [24]; Borishanskij et al. [25]; Bjorge et al. [26]; Kandlikar [27]; Steiner and Taborek [28]; Schrock and Grossman [29]; Zhao et al. [9]) in Figs. 8, 9 and 10, while the statistical comparison between measured data and the predictions of these correlations is reported in Table 2. All these correlations are specific for flow boiling in straight tubes with the exception of the method of Zhao et al. [9], which was specifically derived for helical coils. Further details regarding the implementation of these correlations can be found in the Electronic Annex, available in the online version of this article, while a more comprehensive account of the straight tube correlations can be found in Thome and Cioncolini [30]. As can be seen in Table 2, seven straight tube correlations (Chen [20]; Shah [21]; Gungor and Winterton [22,23]; Liu and Winterton [24]; Bjorge et al. [26] and Kandlikar [27]) fit the present

helical coil databank with a mean absolute percentage error within 15-20%, which is comparable with the experimental uncertainty of the present heat transfer coefficient measurements, which was on the order of 10-20%. Moreover, as can be noticed in Table 2, most of the time these straight tube correlations approximate the measured data from the conservative side, i.e. the straight tube correlations slightly underpredict the helical coil measurements. This may be indicative of enhancement resulting from curvature effects. This effect is however within 5-10% at most, based on the present measurements, too small to be properly resolved with the present experimental apparatus and numerically negligible for most practical applications. Within the limits of the present study, therefore, curvature effects on flow boiling heat transfer in helical coils at low mass flux and low heat flux seem to be at most minimal, and the heat transfer coefficient can therefore be predicted with existing correlations for straight tubes. In particular, the methods of Chen [20], Shah [21], Gungor and Winterton [22,23], Liu and Winterton [24], Bjorge et al. [26] and Kandlikar [27] fit the present data fairly well, and within the limits of the present study can therefore be suggested for general use in design applications. Notably, most of the time these straight tube correlations slightly underpredict helical coil data, and this is normally welcome in both design applications and in transient and safety analysis. In substantial agreement with the present study, the Chen [20] and the Steiner and Taborek [28] straight tube correlations were found to satisfactorily fit helical coils data by Owhadi et al. [6], Zhao et al. [9], Hwang et al. [12] and Chung et al. [11]. It is worth noting that the above conclusions are limited to the heat transfer coefficient *below* the dryout point, as in helical coils the curvature strongly affects the dryout and the post dryout heat transfer (Owhadi et al. [6], Hwang et al. [12]).

4. Conclusions

The heat transfer coefficient during flow boiling of water in an electrically heated, full-scale helical coil steam generator tube was measured, covering operating pressures in the range of 2 to 6 MPa, mass fluxes from 200 to 800 $kgm^{-2}s^{-1}$ and heat fluxes from 40 to 230 kWm^{-2}, conditions which are of interest for the design and operation of compact steam generators in nuclear power applications. Overall, 1575 peripherally averaged and axially local heat transfer coefficient measurements were collected, with an experimental uncertainty within 5-20%. The heat transfer coefficient was found to depend on the mass flux and the heat flux, indicating that both nucleate boiling and convection are contributing to the heat transfer. Curvature effects on the heat transfer during flow boiling were found to be small and negligible, so that the heat transfer coefficient in helical coils can be predicted for design applications with existing correlations for straight tubes, such as the methods of Chen [20], Shah [21],

Gungor and Winterton [22,23], Liu and Winterton [24], Bjorge et al. [26] and Kandlikar [27]. Notably, the majority of these straight tube correlations tend to slightly underpredict helical coil data.

Nomenclature

d	tube diameter (m)
D	coil diameter (m)
f	Fanning friction factor (-)
Nu	Nusselt number (-)
Pr	Prandtl number evaluated at fluid bulk temperature (-)
Pr_w	Prandtl number evaluated at inner tube wall temperature (-)
Re	Reynolds number (-)
μ	fluid viscosity at fluid bulk temperature (kg m^{-1} s^{-1})
μ_w	fluid viscosity at inner tube wall temperature (kg m^{-1} s^{-1})

Acknowledgment

SIET Labs staff is gratefully acknowledged for the technical help during the design and the realization of the test facility and the carrying out of the experiments.

Figure captions:

Fig. 1. Schematic representation of the test facility.

Fig. 2. Schematic representation of the test section.

Fig. 3. Experimental results for single-phase heat transfer.

Fig. 4. Measured results from a typical flow boiling test (mass flux: 206 $kgm^{-2}s^{-1}$, heat flux: 51 kWm^{-2}): pressure profile (top), temperature profiles (middle) and heat transfer coefficient profile (bottom).

Fig. 5. Selected histograms describing the experimental data (1575 data points).

Fig. 6. Measured heat transfer coefficient values vs. vapor quality for different mass fluxes and heat fluxes (operating pressure: 6 MPa).

Fig. 7. Measured heat transfer coefficient values vs. vapor quality for different operating pressures (mass flux: 820 $kgm^{-2}s^{-1}$, heat flux: 200 kWm^{-2}).

Fig. 8. Heat transfer coefficient: measured data vs. predictions.

Fig. 9. Heat transfer coefficient: measured data vs. predictions.

Fig. 10. Heat transfer coefficient: measured data vs. predictions.

References

[1] IAEA, Innovative Small and Medium Sized Reactors: Design Features, Safety Approaches and R&D Trends, Tech. Rep. IAEA-TECDOC-1451, International Atomic Energy Agency, 2005.

[2] IAEA, Advances in Small Modular Reactor Technology Developments. A supplement to: IAEA Advanced Reactor Information System (ARIS), International Atomic Energy Agency, 2014.

[3] H. Hidayatullah, S. Susyadi, M.H. Subki, Design and technology development for small modular reactors – Safety expectations, prospects and impediments of their deployment, Prog. Nucl. Energ. 79 (2015) 127-135.

[4] M. Cooper, Small modular reactors and the future of nuclear power in the United States, Energy Res. Soc. Sci. 3 (2014) 161-177.

[5] Z. Liu, J. Fan, Technology readiness assessment of small modular reactor (SMR) designs, Prog. Nucl. Energ. 70 (2014) 20-28.

[6] A. Owhadi, K.J. Bell, B. Crain, Forced convection boiling inside helically-coiled tubes, Int. J. Heat Mass Transfer 11 (1968) 1779-1793.

[7] M. Kozeki, H. Nariai, T. Furukawa, K. Kurosu, A study of helically coiled tube once-through steam generator, Bull. JSME 13 (1970) 1485-1494.

[8] H. Nariai, M. Kobayashi, T. Matsuoka, Friction pressure drop and heat transfer coefficient of two-phase flow in helically coiled tube once-through steam generator for integral type marine water reactor, J. Nucl. Sci. Technol. 19 (1982) 936-947.

[9] L. Zhao, L. Guo, B. Bai, Y. Hou, X. Zhang, Convective boiling heat transfer and two-phase flow characteristics inside a small horizontal helically coiled tubing once-through steam generator, Int. J. Heat Mass Transfer 46 (2003) 4779-4788.

[10] S. Wongwises, M. Polsongkram, Evaporation heat transfer and pressure drop of HFC-134a in a helically coiled concentric tube-in-tube heat exchanger, Int. J. Heat Mass Transfer 49 (2006) 658-670.

[11] Y.J. Chung, K.H. Bae, K.K. Kim, W.J. Lee, Boiling heat transfer and dryout in helically coiled tubes under different pressure conditions, Ann. Nucl. Energy 71 (2014) 298-303.

[12] K.W. Hwang, D.E. Kim, K.H. Yang, J.M. Kim, M.H. Kim, H.S. Park, Experimental study of flow boiling heat transfer and dryout characteristics at low mass flux in helically-coiled tubes, Nucl. Eng. Des. 273 (2014) 529-541.

[13] A. Cioncolini, L. Santini, An experimental investigation regarding the laminar to turbulent flow transition in helically coiled pipes, Exp. Therm. Fluid Sci. 30 (2006) 367-380.

[14] A. Cioncolini, L. Santini, On the laminar to turbulent flow transition in diabatic helically coiled pipe flow, Exp. Therm. Fluid Sci. 30 (2006) 653-661.

[15] A. Cioncolini, L. Santini, M.E. Ricotti, Effects of dissolved air on subcooled and saturated flow boiling of water in a small diameter tube at low pressure, Exp. Therm. Fluid Sci. 32 (2007) 38-51.

[16] A. Cioncolini, L. Santini, M.E. Ricotti, Subcooled and saturated water flow boiling pressure drop in small diameter helical coils at low pressure, Exp. Therm. Fluid Sci. 32 (2008) 1301-1312.

[17] L. Santini, A. Cioncolini, C. Lombardi, M.E. Ricotti, Two-phase pressure drops in a helically coiled steam generator, Int. J. Heat Mass Transfer 51 (2008) 4296-4239.

[18] L. Santini, A. Cioncolini, C. Lombardi, M.E. Ricotti, Dryout occurrence in a helically coiled steam generator for nuclear power application, EPJ Web Conf. 67 (2014) 02102.

[19] V. Gnielinski, Helically coiled tubes of circular cross section, in: G.F. Hewitt (Ed.), HEDH-Heat Exchanger Design Handbook, Vol. 2, Begell House, New York, 2008.

[20] J.C. Chen, Correlation for boiling heat transfer to saturated fluids in convective flow, Ind. Eng. Chem. Proc. Des. 5 (1966) 322-329.

[21] M.M. Shah, Chart correlation for saturated boiling heat transfer: equations and further study, ASHRAE Trans. 88 (1982) 185-196.

[22] K.E. Gungor, R.H.S Winterton, A general correlation for flow boiling in tubes and annuli, Int. J. Heat Mass Transfer 29 (1986) 351-358.

[23] K.E. Gungor, R.H.S Winterton, Simplified general correlation for saturated flow boiling and comparison of correlations with data, Chem. Eng. Res. Des. 65 (1987) 148-156.

[24] Z. Liu, R.H.S. Winterton, A general correlation for saturated and subcooled flow boiling in tubes and annuli based on a nucleate pool boiling equation, Int. J. Heat Mass Transfer 34 (1991) 2759-2766.

[25] B.M. Borishanskij, A.A. Andreevskij, V.N. Fromzel, B.S. Fokin, V.A. Cistgakov, G.N. Danilowa, G.S. Bikov, Heat transfer during two-phase flows, Teploenergetika 11 (1971) 68-69.

[26] R.W. Bjorge, G.R. Hall, W. Rohsenow, Correlation of forced convection boiling heat transfer data, Int. J. Heat Mass Transfer 25 (1982) 753-757.

[27] S.G. Kandlikar, A general correlation for saturated two-phase flow boiling heat transfer inside horizontal and vertical tubes, ASME J. Heat Transfer 112 (1990) 219-228.

[28] D. Steiner, J. Taborek, Flow boiling heat transfer in vertical tubes correlated by an asymptotic model, Heat Transfer Eng. 13 (1992) 43-69.

[29] V.E. Schrock, L.M. Grossman, Forced convection boiling studies, Univ. California, Inst. Eng. Res. Berkeley, Final report Ser. No. 73308-UCX 2182, TID-14632 (1959).

[30] J.R. Thome, A. Cioncolini, Flow Boiling in Macro and Microchannels, Vol. 3, Set 1, in: Encyclopedia of Two-Phase Heat Transfer and Flow, World Scientific Publishing, Singapore, 2015.

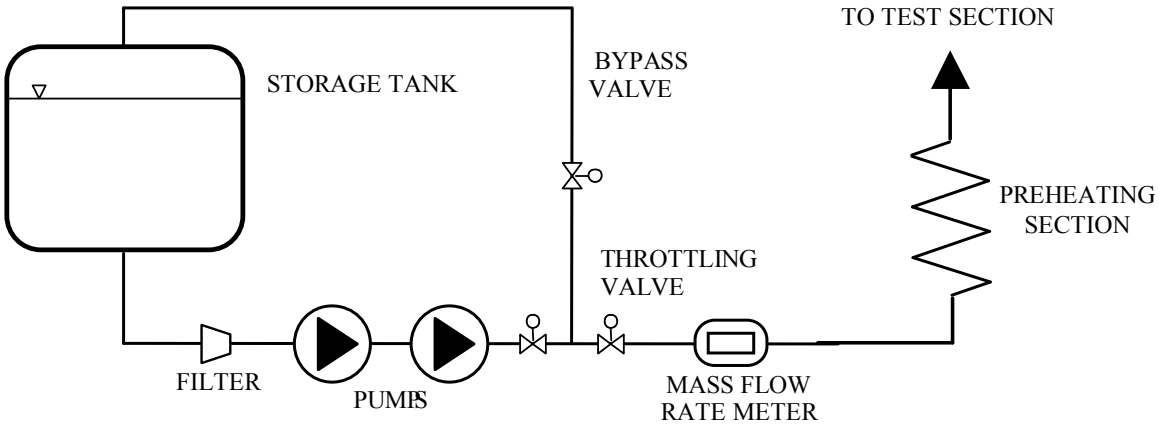

Fig. 1. Schematic representation of the test facility.

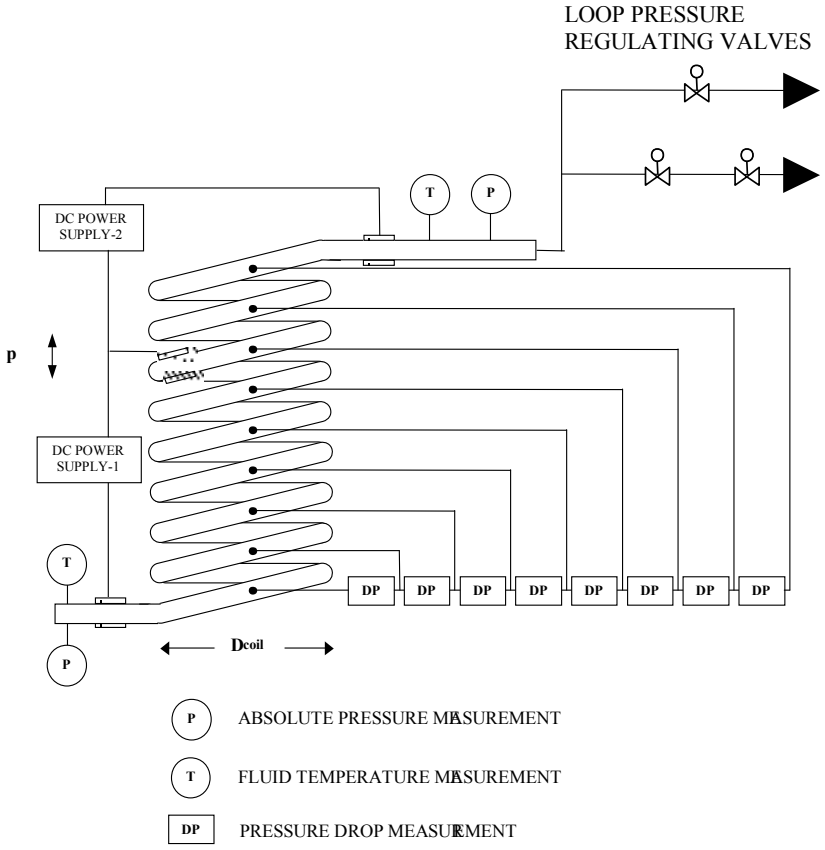

Fig. 2. Schematic representation of the test section.

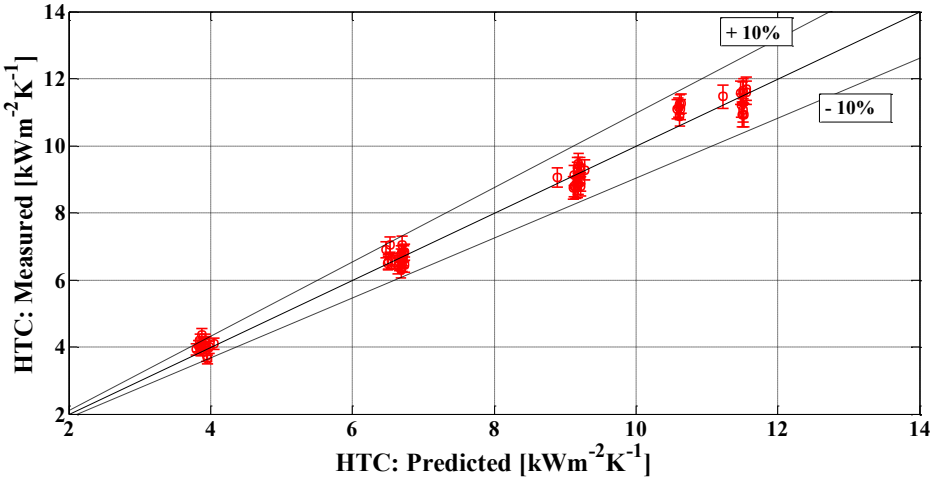

Fig. 3. Experimental results for single-phase heat transfer.

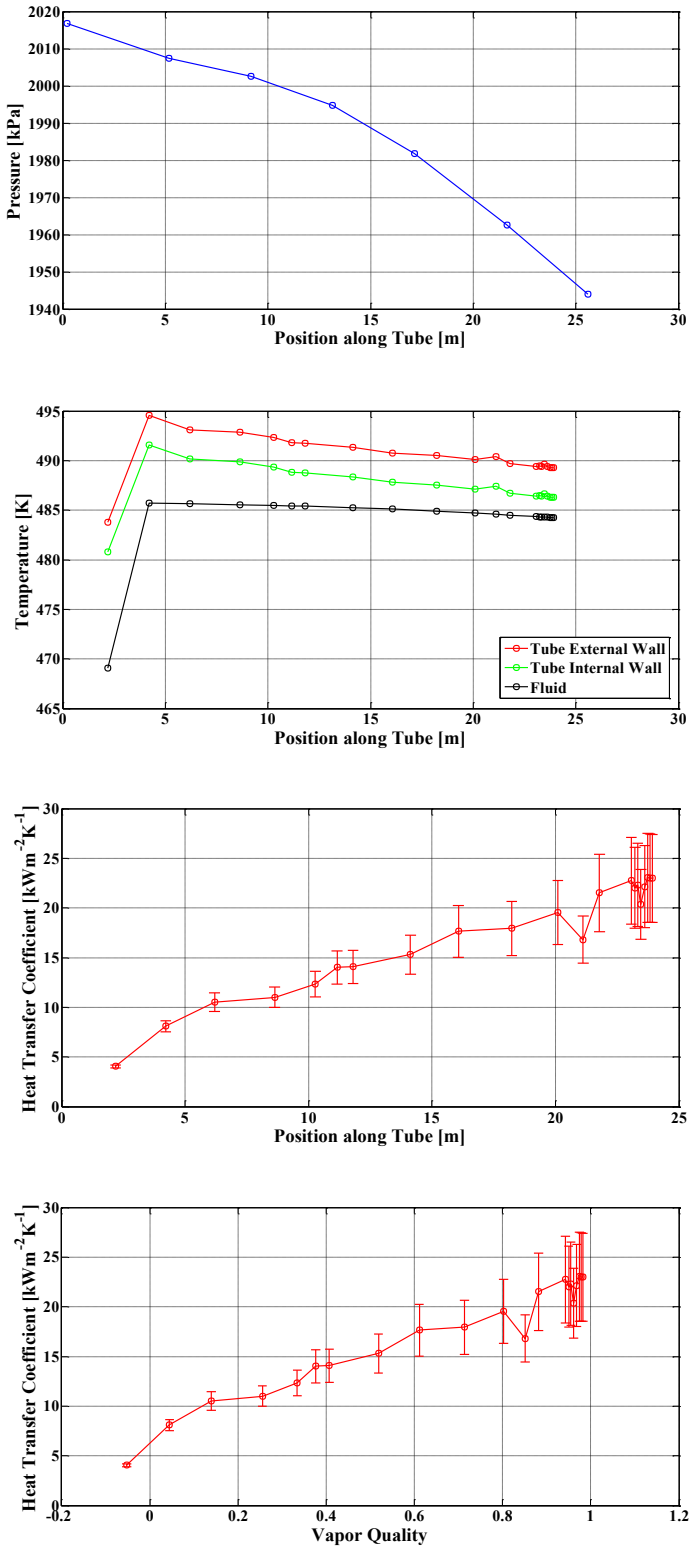

Fig. 4. Measured results from a typical flow boiling test (mass flux: 206 $kgm^{-2}s^{-1}$, heat flux: 51 kWm^{-2}): pressure profile (top), temperature profiles (middle) and heat transfer coefficient profile (bottom).

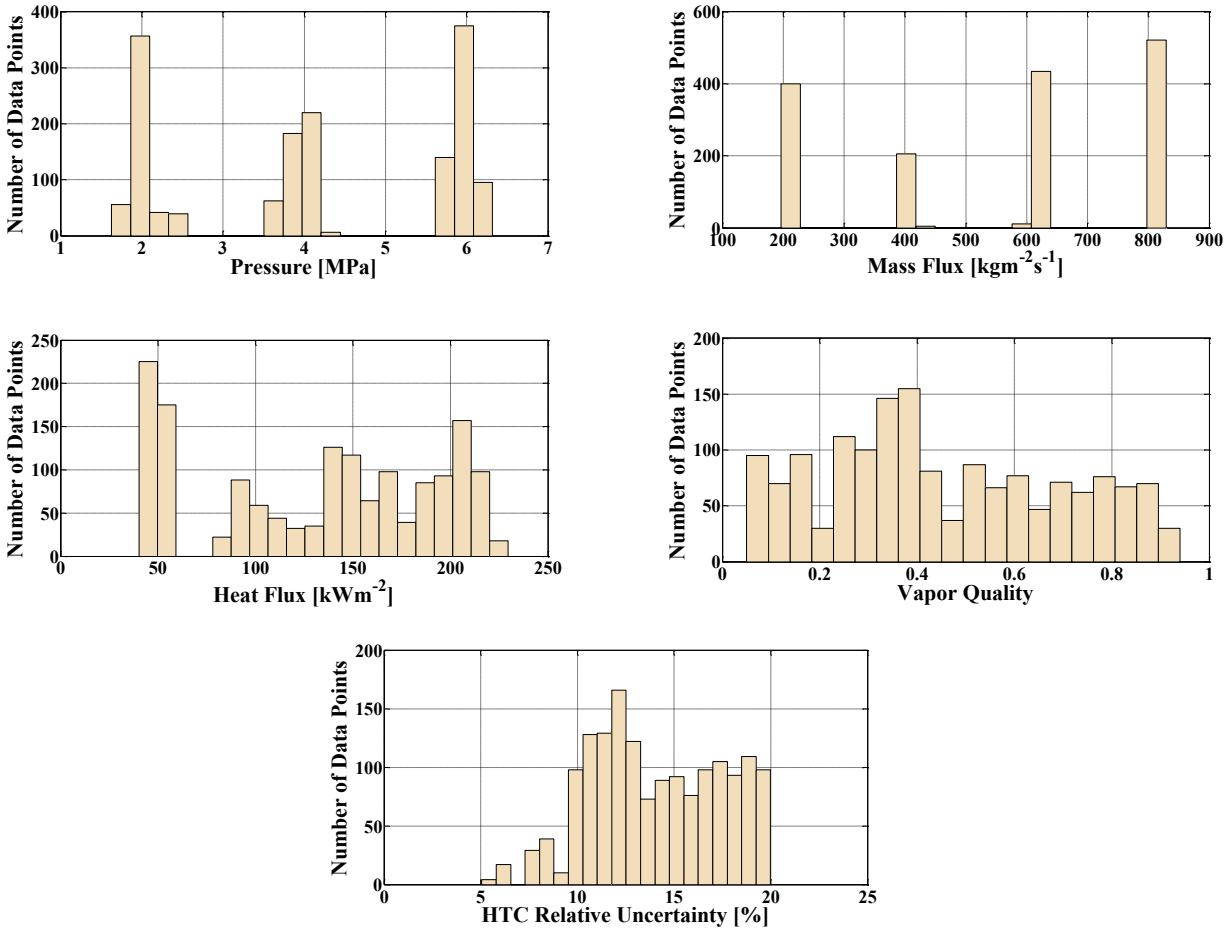

Fig. 5. Selected histograms describing the experimental data (1575 data points).

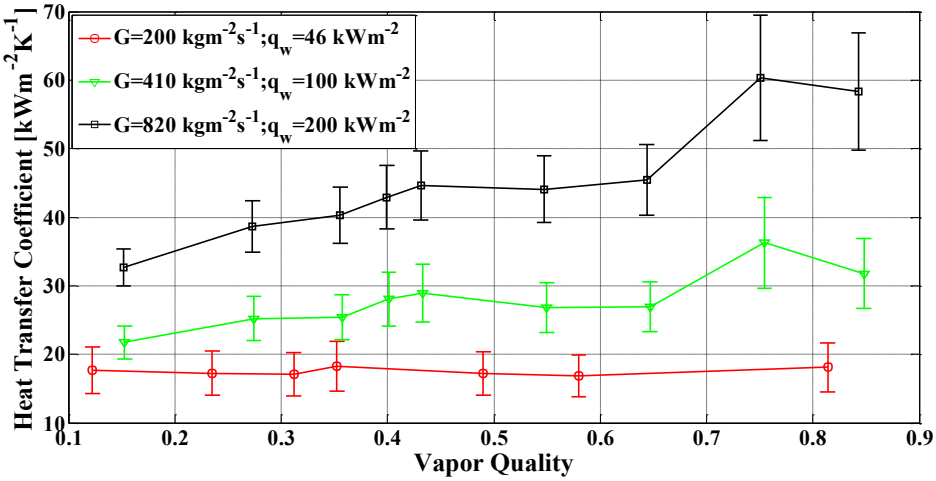

Fig. 6. Measured heat transfer coefficient values vs. vapor quality for different mass fluxes and heat fluxes (operating pressure: 6 MPa).

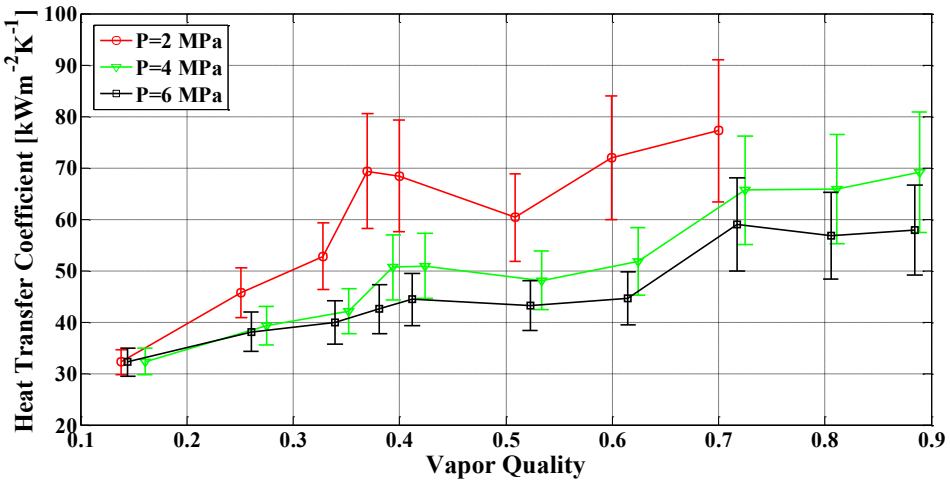

Fig. 7. Measured heat transfer coefficient values vs. vapor quality for different operating pressures (mass flux: 820 $kgm^{-2}s^{-1}$, heat flux: 200 kWm^{-2}).

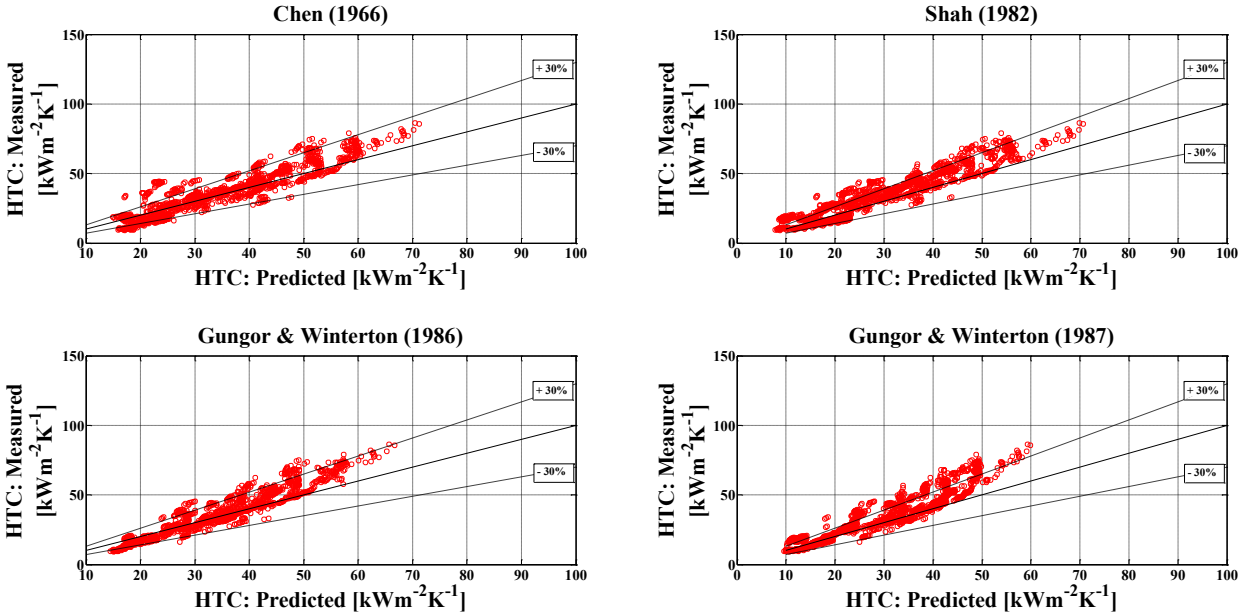

Fig. 8. Heat transfer coefficient: measured data vs. predictions.

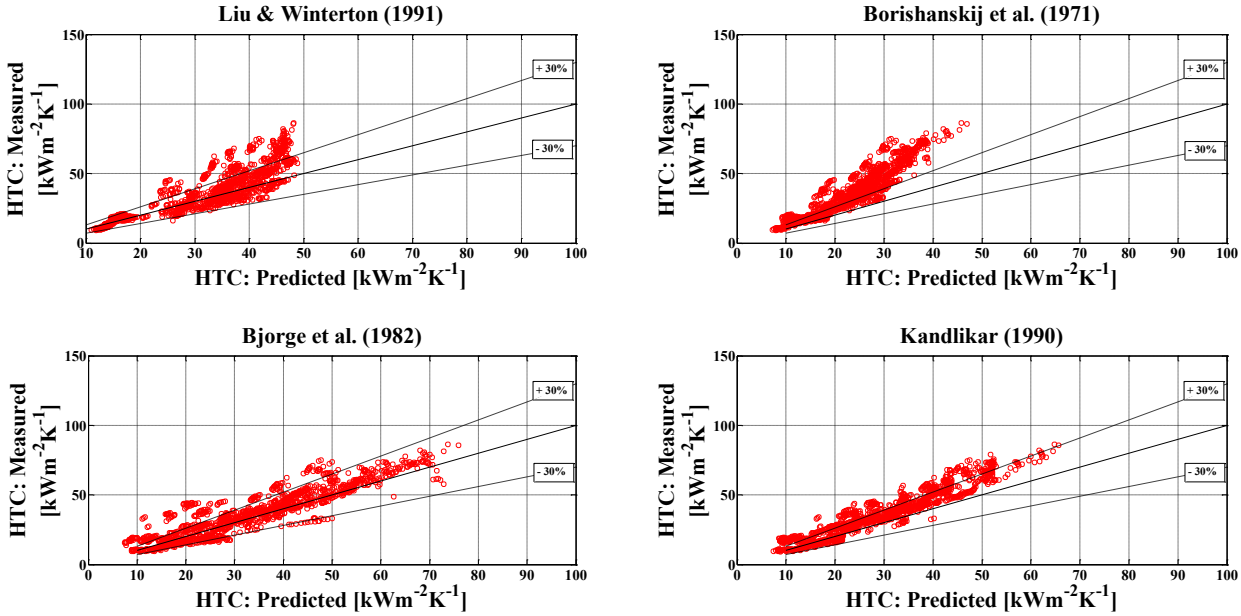

Fig. 9. Heat transfer coefficient: measured data vs. predictions.

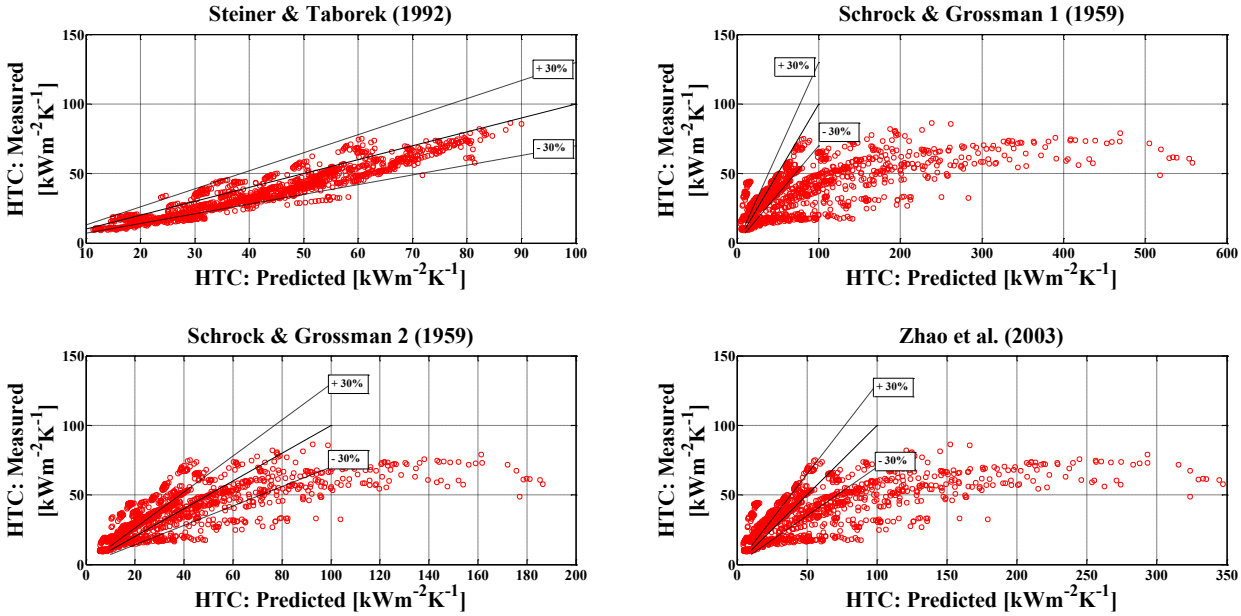

Fig. 10. Heat transfer coefficient: measured data vs. predictions.

Table 1. Test section main geometrical data

Tube internal diameter [mm]	12.49
Tube external diameter [mm]	17.23
Tube internal roughness [μm]	3.1
Coil diameter [m]	1.0
Coil pitch [m]	0.79
Tube length [m]	32.0
Steam generator height [m]	8.0
Number of coil turns	10

Table 2. Statistical comparison between experimental heat transfer data and predictions.

	(1)	(2)	(3)	(4)	(5)
Chen (1966)	17.6	-3.7	60.6	81.8	94.0
Shah (1982)	18.7	12.1	37.1	85.4	99.7
Gungor and Winterton (1986)	15.2	-1.0	58.6	88.7	98.2
Gungor and Winterton (1987)	15.9	11.1	53.6	84.4	99.9
Liu and Winterton (1991)	16.0	6.1	54.0	84.5	99.9
Borishanskij et al. (1971)	31.8	31.7	10.7	43.7	93.7
Bjorge et al. (1982)	16.9	5.0	54.9	82.1	95.2
Kandlikar (1990)	19.7	16.3	36.7	84.1	99.5
Steiner and Taborek (1992)	24.0	-21.1	36.1	71.2	92.5
Schrock and Grossman-1 (1959)	115.7	-103.0	19.4	31.0	46.5
Schrock and Grossman-2 (1959)	34.3	1.9	22.9	56.4	82.0
Zhao et al. (2003)	62.7	-36.7	22.7	42.5	63.4

(1)-Mean absolute percentage error (%) $\frac{100}{n}\sum_{1}^{n}\frac{\left|h_{\exp}-h_{cal}\right|}{h_{\exp}}$

(2)-Mean percentage error (%) $\frac{100}{n}\sum_{1}^{n}\frac{h_{\exp}-h_{cal}}{h_{\exp}}$

(3)-Percentage of experimental data captured within ± 15 %

(4)-Percentage of experimental data captured within ± 30 %

(5)-Percentage of experimental data captured within ± 50 %

Heat transfer coefficient correlations

Before describing the heat transfer coefficient correlations used in the manuscript, some frequently used flow parameters are summarized below.

Liquid-only and liquid-all Reynolds numbers:

$$\mathrm{Re}_{lo} = \frac{G(1-x)\,d}{\mu_l}; \quad \mathrm{Re}_{la} = \frac{G\,d}{\mu_l} \tag{1}$$

Liquid Prandtl number:

$$\mathrm{Pr}_l = \frac{c_{pl}\,\mu_l}{k_l} \tag{2}$$

Liquid-only and liquid-all single-phase heat transfer coefficients:

$$h_{lo} = \frac{k_l}{d} 0.023\,\mathrm{Re}_{lo}^{0.8}\,\mathrm{Pr}_l^{0.4}; \quad h_{la} = \frac{k_l}{d} 0.023\,\mathrm{Re}_{la}^{0.8}\,\mathrm{Pr}_l^{0.4} \tag{3}$$

Turbulent-turbulent Martinelli parameter:

$$\chi_{tt} = \left(\frac{1-x}{x}\right)^{0.9}\left(\frac{\rho_g}{\rho_l}\right)^{0.5}\left(\frac{\mu_l}{\mu_g}\right)^{0.1} \tag{4}$$

Boiling number, convection number and liquid Froude number:

$$Bo = \frac{q_w}{G\,h_{gl}}; \quad Co = \left(\frac{1-x}{x}\right)^{0.8}\left(\frac{\rho_g}{\rho_l}\right)^{0.5}; \quad Fr_l = \frac{G^2}{\rho_l^2\,g\,d} \tag{5}$$

1. Chen (1966):

$$h = F\,h_{lo} + S\,h_b \tag{6}$$

$$F = 1 \quad if \quad \frac{1}{\chi_{tt}} \le 0.1; \quad F = 2.35\left(\frac{1}{\chi_{tt}} + 0.213\right)^{0.736} \quad if \quad \frac{1}{\chi_{tt}} \ge 0.1; \tag{7}$$

$$S = \left[1 + 2.53\cdot 10^{-6}\,(\mathrm{Re}_{lo}\,F^{1.25})^{1.17}\right]^{-1} \tag{8}$$

$$h_b = 0.00122\left(\frac{k_l^{0.79}\,c_{pl}^{0.45}\,\rho_l^{0.49}}{\sigma^{0.5}\,\mu_l^{0.29}\,\rho_g^{0.24}\,h_{gl}^{0.24}}\right)\Delta T_{sat}^{0.24}\,\Delta P^{0.75}; \quad \Delta T_{sat} = T_w - T_{sat}; \quad \Delta P = P(T_w) - P_{sat} \tag{9}$$

2. Shah (1982):

$$h = h_{lo}\max(Fi_{cb}, Fi_2) \tag{10}$$

$$Fi_{cb} = 1.8\, N_s^{-0.8} \tag{11}$$

$$\begin{aligned} Fi_2 &= F_s\, Bo^{0.5} \exp(2.47 N_s^{-0.15}) \quad if \quad N_s \le 0.1; \\ Fi_2 &= F_s\, Bo^{0.5} \exp(2.74 N_s^{-0.1}) \quad if \quad 0.1 \le N_s \le 1; \end{aligned} \tag{12}$$

$$\begin{aligned} Fi_2 &= 230 Bo^{0.5} \quad if \quad N_s \ge 1 \quad and \quad Bo \ge 0.3 \cdot 10^{-4}; \\ Fi_2 &= 1 + 46 Bo^{0.5} \quad if \quad N_s \ge 1 \quad and \quad Bo \le 0.3 \cdot 10^{-4} \end{aligned} \tag{13}$$

$$N_s = Co \quad if \quad Fr_l \ge 0.04; \quad N_s = 0.38 Fr_l^{-0.3} Co \quad if \quad Fr_l \le 0.04 \tag{14}$$

$$F_s = 14.7 \quad if \quad Bo \ge 11 \cdot 10^{-4}; \quad F_s = 15.4 \quad if \quad Bo \le 11 \cdot 10^{-4} \tag{15}$$

3. Gungor and Winterton (1986):

$$h = E\, h_{lo} + S\, h_b \tag{16}$$

$$E = 1 + 2.4 \cdot 10^4\, Bo^{1.16} + 1.37 \chi_{tt}^{-0.86} \tag{17}$$

$$S = \left(1 + 1.15 \cdot 10^{-6} E^2 \,\mathrm{Re}_{lo}^{1.17}\right)^{-1} \tag{18}$$

$$h_b = 55 \left(\frac{P}{P_{cr}}\right)^{0.12} \left(-Log_{10} \frac{P}{P_{cr}}\right)^{-0.55} M^{-0.5} q_w^{0.67} \tag{19}$$

where P_{cr} is the critical pressure and M the molar mass of the fluid.

4. Gungor and Winterton (1987):

Simplified version of the preceding one: the parameter S=0 while the parameter E is now calculated as follows:

$$E = 1 + 3000 Bo^{0.86} + 1.12 \left(\frac{x}{1-x}\right)^{0.75} \left(\frac{\rho_l}{\rho_g}\right)^{0.41} \tag{20}$$

5. Liu and Winterton (1991):

$$h = \left[(F\, h_{la})^2 + (S\, h_{pb})^2\right]^{0.5} \tag{21}$$

The pool boiling heat transfer coefficient h_{pb} is predicted according to Eq. (19), while the forced convection enhancement factor F and the pool boiling suppression factor S are:

$$F = \left\{1 + x\, \mathrm{Pr}_l \left(\frac{\rho_l}{\rho_g} - 1\right)\right\}^{0.35} \tag{22}$$

$$S = \left(1 + 0.055\, F^{0.1}\, \mathrm{Re}_{la}^{0.16}\right)^{-1} \tag{23}$$

6. Borishanskij at al. (1971):

$$h = \sqrt{(h_{lo}^2 + 0.49h_b^2)\left[1 + 7\cdot 10^{-9}\left(\frac{h_b}{\sqrt{h_{lo}^2 + 0.49h_b^2}}\right)^2\left(1 - x\frac{\rho_l - \rho_g}{\rho_g}\right)^{1.5} Bo^{-1.5}\right]} \tag{24}$$

$$h_b = 0.625\left(P^{0.14} + 8.95\cdot 10^{-14}P^2\right)q_w^{0.7} \tag{25}$$

where P is in Pa and q_w in Wm^{-2}.

7. Bjorge at al. (1982):

$$h = \frac{1}{T_w - T_{sat}}\left\{q_{fc} + q_{fdb}\left[1 - \left(\frac{\Delta T_{onb}}{T_w - T_{sat}}\right)^3\right]\right\} \tag{26}$$

$$q_{fc} = F_b \,\mathrm{Pr}_l \frac{k_l}{d}(T_w - T_{sat})\frac{\mathrm{Re}_{lo}^{0.9}}{C_2} \tag{27}$$

$$q_{fdb} = 1.89\cdot 10^{-14}\mu_l h_{gl}\sqrt{\frac{g(\rho_l - \rho_g)}{\sigma}}\left[\frac{k_l^{0.5}\rho_l^{2.125}c_{pl}^{2.375}\rho_g^{0.125}(T_w - T_{sat})^3}{\mu_l h_{gl}^{0.875}(\rho_l - \rho_g)^{1.125}\sigma^{0.625}T_{sat}^{0.125}}\right] \tag{28}$$

$$\Delta T_{onb} = \frac{8\sigma T_{sat} h_{la}}{k_l h_{gl}}\left(\frac{1}{\rho_g} - \frac{1}{\rho_l}\right) \tag{29}$$

$$F_b = 0.15\left(\chi_{tt}^{-1} + 2\chi_{tt}^{-0.32}\right) \tag{30}$$

$$\begin{aligned} &C_2 = 0.0707\,\mathrm{Pr}_l\,\mathrm{Re}_{lo}^{0.5}; \quad if \quad \mathrm{Re}_{lo} \le 50; \\ &C_2 = 5\,\mathrm{Pr}_l + 5\ln\left[1 + \mathrm{Pr}_l\left(0.0964\,\mathrm{Re}_{lo}^{0.585} - 1\right)\right]; \quad if \quad 50 \le \mathrm{Re}_{lo} \le 1125; \\ &C_2 = 5\,\mathrm{Pr}_l + 5\ln\left(1 + 5\,\mathrm{Pr}_l\right) + 2.5\ln\left(0.0031\,\mathrm{Re}_{lo}^{0.812}\right); \quad if \quad \mathrm{Re}_{lo} \ge 1125 \end{aligned} \tag{31}$$

8. Kandlikar (1990)

$$\frac{h_{tpf}}{h_{lo}} = C_1 Co^{C_2}\left(25Fr\right)^{C_5} + C_3 Bo^{C_4} F_{fl} \tag{32}$$

The heat transfer coefficient is calculated for both the convective and nucleate boiling regions using the respective values of C_1-C_5 from the Table below, and the highest calculated coefficient is taken. The Froude number is calculated for the flow as all liquid ($V^2(gd_i)^{-1}$), while F_{fl} is a fluid dependent parameter (equal to 1 for water).

Constants in Eq. (32)

	Convective Region	Nucleate Boiling Region
C_1	1.136	0.6683
C_2	-0.9	-0.2
C_3	667.2	1058.0
C_4	0.7	0.7
C_5 (vertical flow)	0.0	0.0
C_5 (horizontal flow, $Fr > 0.04$)	0.0	0.0
C_5 (horizontal flow, $Fr < 0.04$)	0.3	0.3

9. Steiner and Taborek (1992)

The heat flux required for the onset of nucleate boiling is predicted as:

$$q_{onb} = \frac{2\sigma T_{sat} h_{la}}{R_{cr} \rho_g h_{gl}} \tag{33}$$

Where R_{cr}=0.3 μm. If $q_w < q_{onb}$:

$$h = F h_{la} \tag{34}$$

$$F = \left\{ \left[(1-x)^{1.5} + 1.9 x^{0.6} (1-x)^{0.01} \left(\frac{\rho_l}{\rho_g} \right)^{0.35} \right]^{-2.2} + \left[\frac{h_{ga}}{h_{la}} x^{0.01} \left(1 + 8(1-x)^{0.7} \left(\frac{\rho_l}{\rho_g} \right)^{0.67} \right) \right]^{-2} \right\}^{-0.5} \tag{35}$$

Otherwise:

$$h = \left[(F\, h_{la})^3 + (S\, h_{pb})^3 \right]^{0.33} \tag{36}$$

$$F = \left[(1-x)^{1.5} + 1.9 x^{0.6} \left(\frac{\rho_l}{\rho_g} \right)^{0.35} \right]^{1.1} \tag{37}$$

$$S = \left[2.816 P_r^{0.45} + \left(3.4 + \frac{1.7}{1 - P_r^7} \right) P_r^{3.7} \right] \left(\frac{q_w}{q_0} \right)^{0.8 - 0.1 \exp(1.75 P_r)} \left(\frac{d}{d_0} \right)^{-0.4} \left(\frac{R}{R_0} \right)^{0.133} f(M) \tag{38}$$

Where P_r is the reduced pressure, q_0=150 kWm^{-2} (for water), d_0=0.01m, R is the surface roughness of the tube, R_0=1μm, $f(M)$=0.72 (for water) and h_{pb}=25.58 kWm^{-2}K^{-1} (for water).

10. Schrock and Grossman 1 (1959):

$$h = 2.5\, h_{la}\, \chi_{tt}^{-0.75} \tag{39}$$

11. Schrock and Grossman 2 (1959):

$$h = h_{la}\left(7390Bo + 1.108\chi_{tt}^{-0.667}\right) \tag{40}$$

12. Zhao et al. (2003)

$$h = h_{la}\left(1.8310^{5}Bo^{1.46} + 1.6\chi_{tt}^{-0.74}\right) \tag{41}$$